NUMERICAL INVESTIGATION OF THE THERMAL BENEFIT OF USING A HIGH THERMAL CONDUCTIVITY CMC FOR THE LEADING EDGE OF HYPERSONIC VEHICLES

Thomas Reimer [(1)], Ivaylo Petkov [(1)], Waldemar Rotärmel [(1)]

[(1)] German Aerospace Center DLR, Pfaffenwaldring 38-40, 70569 Stuttgart, Germany
Thomas.Reimer@dlr.de, Ivaylo.Petkov@dlr.de, Waldemar.Rotaermel@dlr.de

ABSTRACT

During atmospheric re-entry high thermal loads are generated on the surface of the entry vehicle with peak loads in the stagnation area. Typical entry vehicles have a blunt shape avoiding sharp tips or leading edges. Recent developments for vehicles in the hypersonic flight regime have concentrated on sharp designs to reduce drag and increase lift. This creates challenges with regard to the materials. Ceramic matrix composites are materials with good high-temperature properties. However, the thermal loads on sharp structures can exceed even their capabilities. One way to relieve the problem could be to use a material with a very high thermal conductivity to distribute the heat load over a wider area and thereby reducing the temperature to an acceptable level. In this work the potential of a new type of CMC material based on the use of carbon pitch fibers was investigated via numerical simulation.

1. INTRODUCTION

High thermal loads are present on the surface of a re-entry vehicle during atmospheric descent with peak loads in the stagnation area. In order to control this, typical entry vehicles have a blunt shape avoiding sharp tips or leading edges. Recent developments to increase the aerodynamic efficiency of such vehicles in the hypersonic flight regime have, however, concentrated on designs that rely especially on slender shapes featuring sharp leading edges to reduce drag and increase lift [1]. This creates challenges with regard to the materials used for the tip or leading edge of the vehicle because heat loads increase with the reduction of the curvature radius [2].

Materials used for the stagnation areas of blunt vehicles with a re-usable TPS were C/C as e.g. for the nose and leading edges of the Space Shuttle [3]. Another Ceramic Matrix Composite (CMC) is C/C-SiC which was used for the X-38 nose [4]. These materials are limited in their maximum use temperature to around 1600-1700° C which is mainly due to the limited performance of protective coatings against oxidation effects. In an attempt to increase the maximum use temperature of such TPS materials Ultra High Temperature Ceramics (UHTC) are proposed for sharp structures and were already flown on test flights e.g. as the SHARP experiments [5,6]. As an alternative method active cooling is investigated and proposed for the leading edge of the SHEFEX vehicle in the form of transpiration cooling [7]. Another option which shall be discussed in this work could be to increase the thermal conductivity of the material used for a tip or leading edge as shown in Fig. 1.
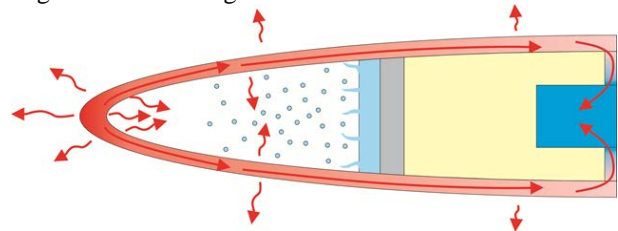

Figure 1. Schematic of the heat load distribution concept

The idea behind this approach is that the heat load on a sharp leading edge is concentrated in a small region around the leading edge and that it is decreasing rapidly when moving downstream. So, if a material with a very high thermal conductivity was available, the heat could be transported from the leading edge to regions with lower heat loads, thereby lowering the temperature of the leading edge.

2. CERAMIC MATRIX COMPOSITE

The CMC which is produced at the Institute of Structures and Design of DLR in Stuttgart is made from carbon fibers which are embedded in a matrix of carbon and silicon carbide and it is thus refered to as C/C-SiC. The fibers are standard industrial grade HT fibers with a relatively low thermal conductivity and so the overall resulting thermal conductivity of the CMC is not very high [8]. The fabrication of C/C-SiC composites at DLR is divided into three steps. In the first step, a carbon fiber reinforced polymer (CFRP) component is produced which can be performed in different ways. The preferred approaches are resin transfer moulding (RTM) or autoclave technology, but warm pressing or filament winding are also accepted processes. After the curing, the composites are tempered for 4 hr at 240° C to complete the polymerization of the matrix. It is essential to use a resin (e.g. phenolic) with high carbon yield in this step to create a matrix with sufficient carbon content in the subsequent step. In the second step, the CFRP composite is pyrolysed under inert

atmosphere (nitrogen) at a temperature of 1650° C to convert the polymer matrix to amorphous carbon. The result is a porous C/C component. The pyrolysis results in a macroscopic shrinkage of about 10% mainly in thickness and a microscopic network of cracks within the C/C composite is formed. The fiber bundles remain practically intact. In the third step, the C/C component is siliconized via melt infiltration. The component is placed into a coated graphite crucible and solid silicon is added as granulated pure metal. After heating up to over 1420° C (melting of silicon) the porous C/C component is filled with liquid silicon due to the capillary effect of the micro-cracks and the low viscosity of the molten silicon. In an exothermic reaction between the molten silicon and the carbon matrix, silicon carbide is formed along the micro cracks encapsulating the carbon fiber bundles. The siliconizing is carried out under vacuum at a temperature of 1650° C. The resulting C/C-SiC composites contain three material phases as shown in Fig. 2. These are the carbon phase (black/dark grey) consisting of carbon fibers and residual carbon matrix, silicon carbide (light gray) as the main matrix constituent and a small share of unreacted free silicon (white).
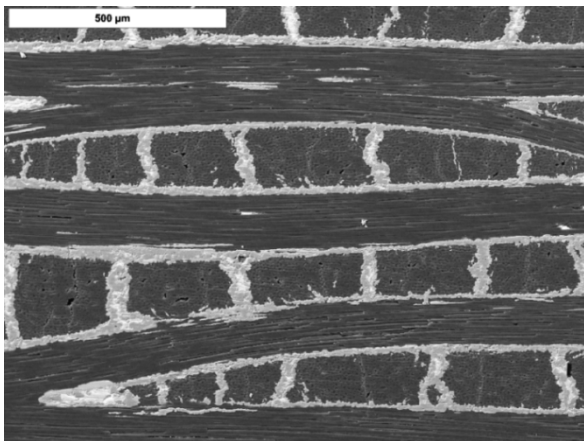

Figure 2. C/C-SiC microstructure

3. PITCH FIBRES

There are three general classes of carbon fibers with regard to their manufacturing and precursors. First, there are the PAN fibers made by processing polyacrylnitril. Second, there are the pitch-based fibers made by processing pitch and last there are fibers produced from Rayon [9]. The conductivity of carbon fibers depends on the degree of orientation of the carbon molecules in the fiber relative to the longitudinal axis. This goes along with the mechanical property of the Young's modulus which is increasing with higher orientation. Pitch fibers can be graphitized to a higher degree than PAN fibers. This increases the thermal conductivity considerably. Pitch fibers with a thermal conductivity of up to 1000 W/mK are available on a lab scale compared to 15 W/mK for the currently used

PAN-based HT fibers [10]. For this study, processing investigations were made to fabricate a high-conductivity CMC via melt infiltration technology using pitch fibers. The fibers that were selected for the investigations were two types, namely the Mitsubishi K63A12 and the Nippon Graphite NGF SF-YS95A-100 fiber with a thermal conductivity of 220 W/mK and 600 W/mK respectively.

4. METHODOLOGY

A parametric numerical study was carried out with a generic leading edge geometry to determine the influence of different material variants on the surface temperature with respect to their conductivity. As the baseline geometry and heat load profile, the leading edge section of the SpaceLiner vehicle and the corresponding reference trajectory were selected. The objective was to determine the maximum achievable flight velocity for a given set of geometry and material data with the constraint of not exceeding a maximum surface temperature that was regarded as the material limit in order to avoid erosion and to be re-usable. The design parameters included the thermal conductivity of the CMC material, the fiber orientation in the cross section of the leading edge, the internal heat exchange via radiation in the leading edge as well as an additional thermal bridge to a cooled structure in the rear of the leading edge section. A numerical model was developed to predict the CMC thermal properties from the available carbon pitch fiber data and the existing data of the standard C/C-SiC ceramic matrix composite. In addition manufacturing studies were carried out to determine the actual physical properties of the pitch fiber CMC and the simulations were repeated with the real data and compared to the predictions.

5. THERMAL CONDUCTIVITY MODELING

The thermal conductivity of a potential pitch fiber CMC was estimated via two different models. First, a material model was set up similar to the way it is done in electric circuit calculations. A block model and the corresponding block diagram were developed that accounts for the thermal resistances of the constituents of the material as there are matrix and fibres in different directions presented in Fig. 3. and Fig. 4.
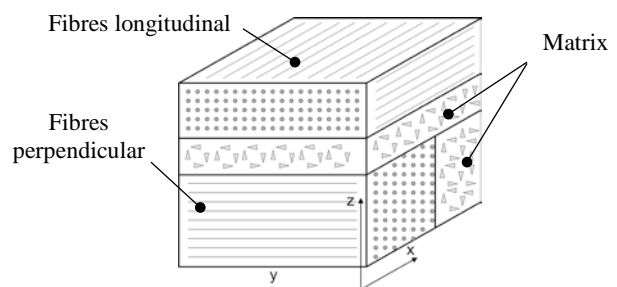

Figure 3. Block model of the CMC constituents

For both material phases the relevant thermal conductivities were specified and the resulting overall conductivity was calculated. For the carbon fibers the conductivity was given as the conductivity along the fibre axis and perpendicular to it.
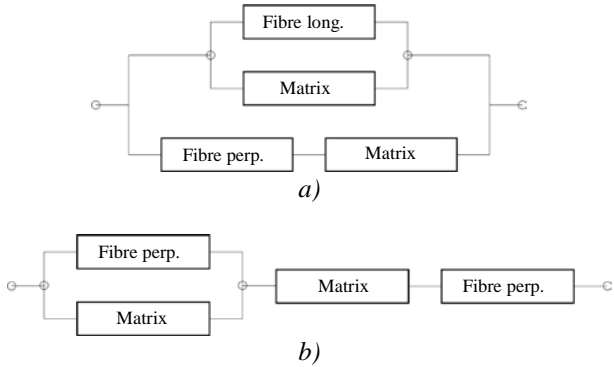

Figure 4. Block diagrams for a) in-plane direction b) out-of-plane direction

In addition a finite elemente model was developed describing the actual geometry of the CMC microstructure in better detail. A unit cell of the microstructure was modelled with detailed fibre bundles as shown in Fig. 5 and Fig. 6.
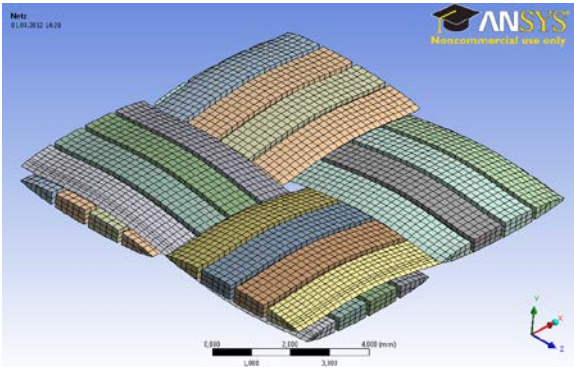
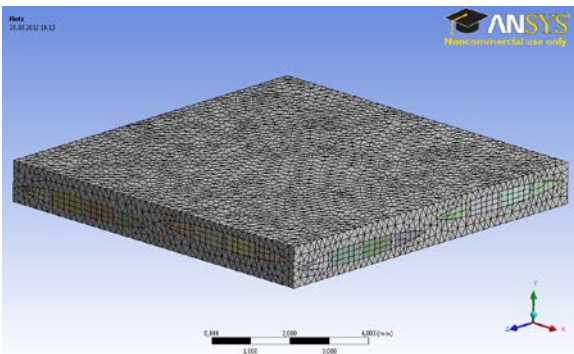

Figure 5. Fibre bundles of the unit cell FE model

Figure 6. FE model of the CMC structure

The thermal conductivity was calculated using both approaches from the block model and from the FE model. The results are given in Fig. 7 and Fig. 8.
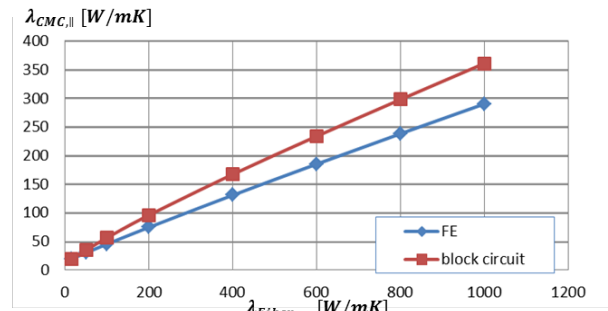

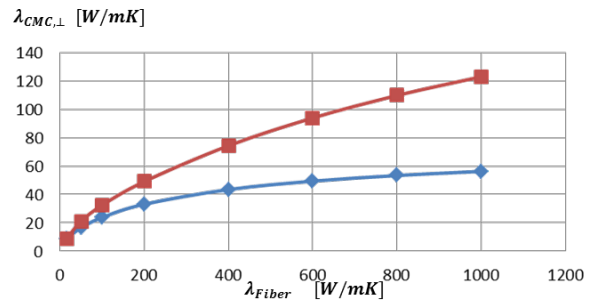*Figure 7. Predicted in-plane thermal conductivity*

Figure 8. Predicted out-of-plane thermal conductivity

6. PITCH FIBER CMC MANUFACTURING

Fabrication trials were carried out with pitch fibers to produce CMC samples in order to measure the real material data for the pitch fiber CMC. The sample manufacturing and the measurement of the properties is in detail described in [11]. Here, the most relevant results are presented which is the temperature dependent thermal conductivity of three different samples shown in Fig. 9. The data was collected from 100° C upward up to 900° C. At 100° C the thermal conductivity is between 94 and 155 W/mK. The plates IP 521 and IP 523 were made with the Mitsubishi fiber K63A12 (220 W/mK), the plate IP 527 was made with the NGF fiber SF-YS-9-A (600 W/mK).
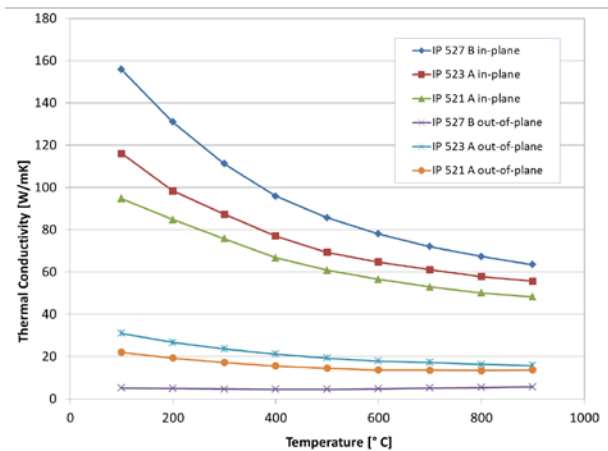

Figure 9. Thermal conductivity of pitch fiber samples

The room temperature conductivity prediction for a CMC using a fiber of 220 W/mK was approximately 100 W/mK, that was reached. The RT conductivity prediction for a CMC using a fiber of 600 W/mK was approximately 180 W/mK, which was also reached when the measured data is extrapolated back to RT. However, the measured data shows a strong dependency on the temperature with falling conductivity values over increasing temperature. At 900° C the in-plane values have decreased to between 50 and 65 W/mK. This will be of some importance in the following.

7. LEADING EDGE MODEL

The leading edge of the SpaceLiner vehicle was modelled in ANSYS Workbench. Two models were generated. First, a shell model was worked out to determine the effects of the pitch fibres in a radiation adiabatic condition with no heat transport into the structure. Second, a 3-D geometry was modelled that included the actual thickness of the wing section and accounted for internal heat transport and thermal radiation inside the wing section.
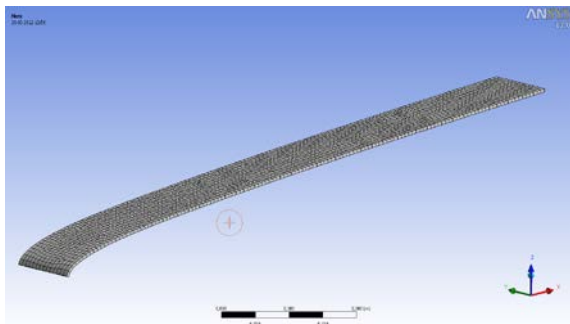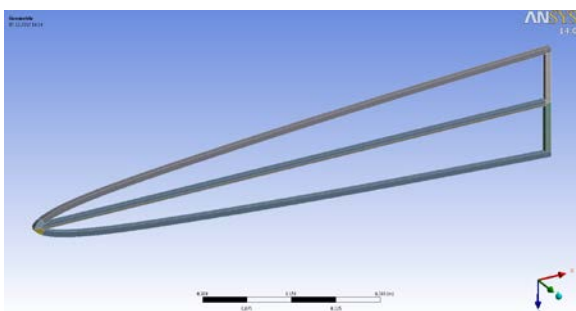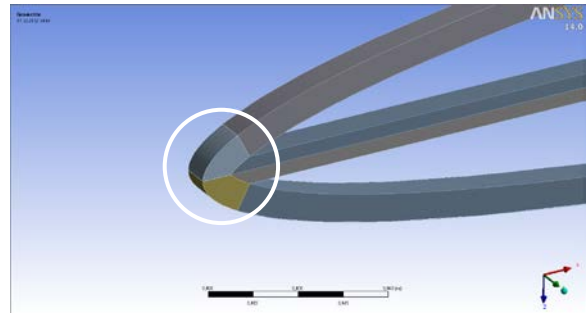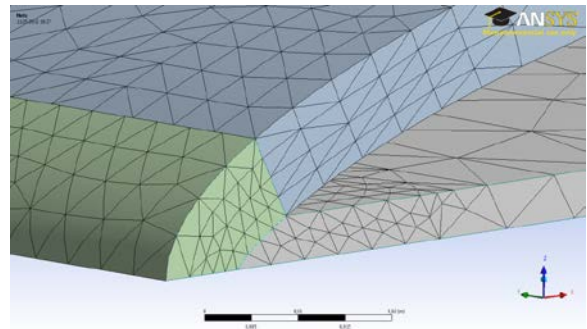

Figure 10. Shell model.

The wing profile is a NACA section. For the purpose of this work a wing depth of 1 m was modelled which is shown in Fig. 10. The thickness of the wing shell was assumed to be 10 mm.

a)

b)

c)

Figure 11. a) 3-D volume model b) nose region with volume to adapt fiber orientation c) mesh

The 3-D volume model shown in Fig. 11 included a structural connection between the nose and the back to simulate a heat bridge between the hot part of the leading edge and the cooler regions. This geometric element could be blanked out during the several simulation runs to determine its effect. At the tip of the model a specific volume was created that was used to be able to change the fibre orientation independently of the aft part of the profile shell.

8. LOADS

The thermal loads for the simulations were derived from the SpaceLiner 7 trajectory depicted in Fig. 12. The SpaceLiner is a generic conept developed by DLR to investigate mission and system aspects of long range passenger transport in space [12].
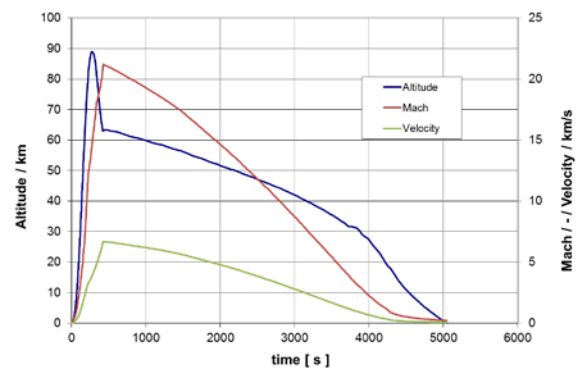

Figure 12. SpaceLiner 7 trajectory

From the trajectory the stagnation heat load was calculated as cold wall heat flux using the DKR approach. From that the hot wall heat flux was calculated with an iterative approach. The distribution over the wing section was approximated applying the cosine law of the local wing section point relative to the flow direction.

The method was verified via a Navier-Stokes CFD simulation with the DLR code TAU at the velocity of Mach 6. For that flight point there was a good agreement between the analytical and the numerical result shown in Fig. 13.
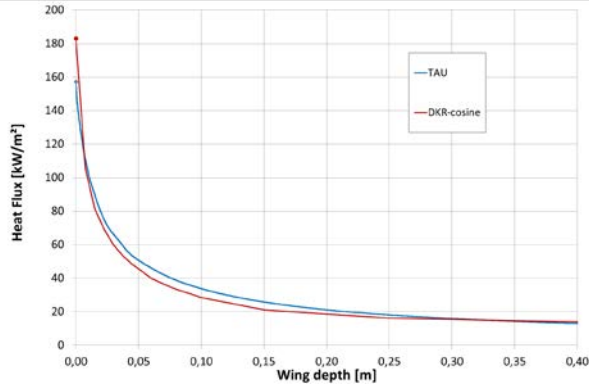

Figure 13. Comparison of the heat load distribution over the leading edge at Ma 6

9. SIMULATION RESULTS

In order to assess the potential of a CMC with very much improved thermal conductivity, the simulations were conducted with the predicted material properties first. The thermal conductivity properties were assumed to be constant over temperature as this is the case with the presently manufactured C/C-SiC. These results are presented in this section. As was shown above, this assumption did not hold when the conductivity was measured and a comparison with simulation results based on the measured data is also presented in the following.

9.1. Simulations with predicted material properties

In a first effort the shell model was employed to simulate radiation adiabatic conditions and evaluate the effects without heat transport into the structure.

Steady state conditions for different Mach numbers between 3 and 21 were simulated as listed in Table 1. In the following, results are mainly discussed for the Ma=10 case. These conditions were also used for the simulations with the 3-D volume model.

Table 1. Simulated Mach numbers and fiber properties

Mach	3, 4, 6, 8, 10, 12, 15, 20, 21
λ_{Fiber} [W/mK]	15, 50, 100, 200, 400, 600, 800, 1000

The condition at the flight velocity of Ma=10 is selected

for the discussion. It is of interest because the resulting temperatures at the stagnation point are around the limit temperature of the material and the goal was to see whether a reduction below the allowable temperature limit can be achieved via alternative fibres.

Depending on the fibre conductivity, the stagnation point temperature reaches values between 1602° C (fibres with 1000 W/mK) and 1851° C (presently used fibres with 15 W/mK) as shown in Fig. 14.
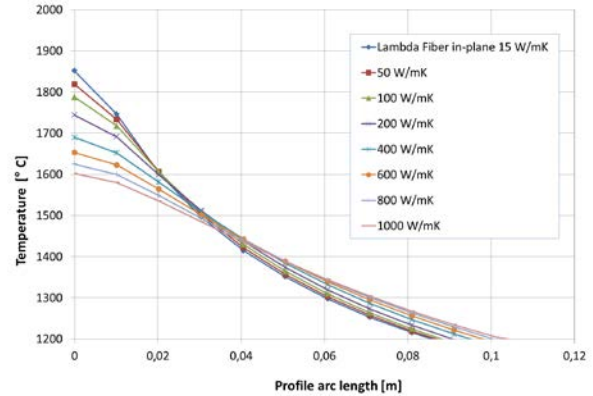

Figure 14. Temperature distribution over the front section of the profile at Ma=10 for the reference case with radiation adiabatic hot wall

Most of the temperature reduction effect occurs in a very small region close to the actual leading edge/stagnation point extending over 3-4 cm to the back. At about 3 cm from the stagnation point there is no temperature change and behind this location temperatures increase slightly due to the additional heat transported there from the stagnation area.

In order to include the geometry effects into the simulation the 3-D volume model was used. Different cases were simulated in terms of the geometry of the front wing section and in terms of physical effects included and in terms of material properties. Table 2 gives an overview about the parameters that were used and varied for the simulations. The case A1 would represent the radiation adiabatic state and was not simulated with the volume model.

Table 2. Analysis parameters

Parameter	Analysis			
	A2	A3	A4	A5
Heat transport inwards	x	x	x	x
Internal radiation cavity	x	x	x	x
Additional internal heat conducting structures		x		x
Adaptation of the fiber orientation at the stagnation point			x	x

The additional simulation parameters were activated step by step to determine their respective influence. In Fig. 15 to 18 the results for different parameter sets are presented. The heating conditions represent the Ma=10 velocity and in order to emphasize the effects, the presented figures are the results for fibers with the highest conductivity of 1000 W/mK.

In Fig. 15 the inward heat transport is activated and internal radiation heat exchange is possible, case A2. The stagnation temperature is 1572° C.

In Fig. 16 the horizontal structure acting as a heat bridge to the colder sections is included in addition representing case A3. This reduces the stagnation temperature to 1541° C.
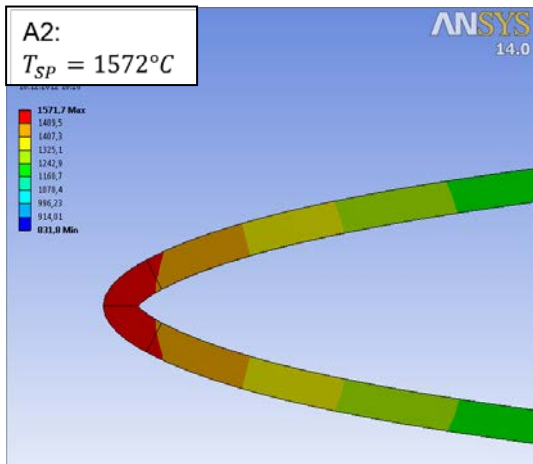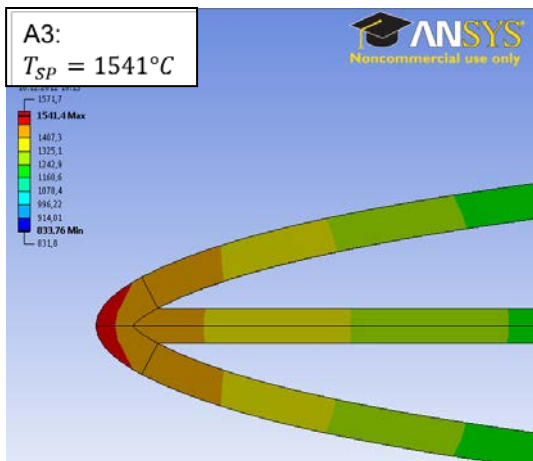

Figure 15. Analysis A2; Ma=10; λ_F=1000W/mK

Figure 16. Analysis A3; Ma=10; λ_F=1000W/mK

In Fig. 17 the fibre orientation in the stagnation region is adapted to the direction of the heat transport. In the previous cases the fibre direction was oriented parallel to the surface of the profile along the shell to transport the heat to the rear of the wing. However, in the stagnation region the temperature gradient is mainly through the thickness of the material. So it is more effective to orient the fibers along the shell normal in order to make better use of the material thickness. The stagnation temperature is 1544° C which has to be compared to the case A2 where 1572° C was reached.

When the same adaptation is done for the configuration with the heat bridge the case A5 is simulated. In that case the stagnation temperature is 1505° C, the lowest of all the different configurations shown in Fig. 18. This compares to A3 where the maximum was 1541° C.

Summarizing the results for the theoretical fiber properties, the internal heat exchange, the heat bridge and the orientation of the fibres in the stagnation region each yield approximately 30 degrees temperature reduction in the stagnation point, getting down the temperature from 1602° C to 1505° C.
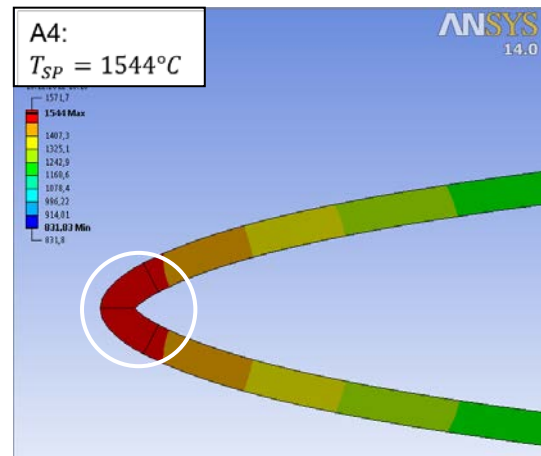

Figure 17. Analysis A4; Ma=10; λ_F=1000W/mK; circle: adaptation of fiber orientation

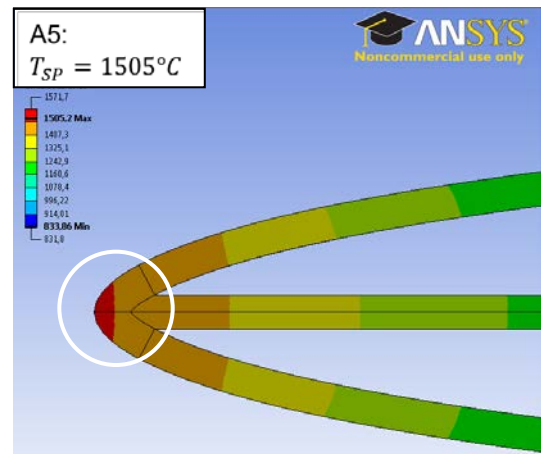*Figure 18. Analysis A5; Ma=10; λ_F=1000W/mK; circle: adaptation of fiber orientation*

When the real material data is used in the simulation the results change and the achieved temperature reductions are smaller which is detailed in Table 3.

Table 3. Stagnation point temperatures for Ma=10

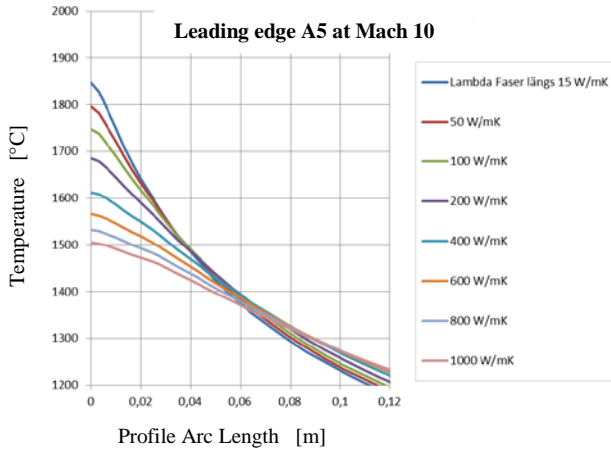| Mach 10		Temp$_{SP}$ [° C]	
		λ$_{Fiber}$ 15 W/mK	λ$_{Fiber}$ 1000 W/mK
A2	no heat bridge internal radiation	1867	1572
A3	with heat bridge	1865	1541
A4	no heat bridge/with adaptation of fibre orientation in SP	1851	1544
A5	with heat bridge/with adaptation of fibre orientation in SP	1848	1505

Figure 19. Temperature distribution over the profile for case A5 at Ma=10 and for different fiber conductivities

In Fig.19 the influence of the fibre quality on the achievable temperature reduction is illustrated. From that results it can be determined which fibre quality and thus CMC conductivity is required to lower the stagnation temperature for a given flight condition under the allowable limit. When e.g. for this material a limit of 1600° C is assumed, the required fibre quality in terms of thermal conductivity to achieve acceptable temperatures at Ma=10 would be approximately 400 W/mK.

9.2. Simulation results with measured material properties

When the simulations are repeated with the actually measured thermal conductivity of the pitch fibre CMC the picture changes considerably. As was described, the thermal conductivity of the CMC is strongly temperature dependent. When these properties are used for the simulations the effects of the temperature reduction at high temperature are much less pronounced.

Since the thermal conductivity decreases with temperature the beneficial effect diminishes the higher

the temperatures get which is counterproductive to the intention.

In Table 4 the results of the simulations with the measured data are summarized for the Mach 10 flight condition and juxtaposed to the results obtained for the predicted material data. Since the conductivity measurements could only be done up to 900° C, the value obtained for 900° C was assumed constant for the simulations. Fig. 9 shows that the conductivity values do in fact further decrease to even lower numbers. The stagnation temperature reduction is much less compared to the initial simulations. For the Mitsubishi fibers a reduction of only 24° C can be achieved, in the case of the NGF fibers the reduction is 39° C.

Table 4. Comparison of stagnation temperatures for Ma=10 between predicted and measured CMC thermal conductivity

λ$_{Fiber}$	T$_{SP}$	T$_{SP}$
	Predicted conductivity	Measured conductivity
[W/mK]	° C	° C
15	1848	1848
200	1686	
220 (Mitsubishi)		1824
600	1565	1809 (NGF)
1000	1505	

10. CONCLUSION

The high thermal conductivity of the carbon pitch fibres is promising for thermal applications. The thermal conductivity of the C/C-SiC which is produced at DLR at the moment is not exceptionally high, it is around 15-20 W/mK in-plane. Therefore for certain applications where localized heat peaks on thermal protection systems occur the development of a highly conductive CMC is intriguing to level out the peak and limit the temperatures to acceptable levels.

A problem is that the thermal conductivity of the pitch fibres is strongly temperature dependent and decreases with increasing temperature. This behaviour can thus also be found in the CMC. At room temperature the conductivity of the CMC could be improved by a factor of 10 from 18 to 180 W/mK for certain fibre types. However, at high temperature there is only a moderate increase in conductivity left. At 900° C the values are around 60 W/mK in the in-plane direction which is a factor of 4 compared to the standard material.

Especially the expectations of a considerable improvement of the thermal conductivity of the C/C-SiC material at high temperature could not be realized. Therefore the effect of a temperature reduction at localized hot spots is small. The simulations with the measured material data only result in a temperature

reduction of 39° C at the stagnation point of the leading edge for the flight condition at Ma=10 for the discussed example of the SpaceLiner.

In light of these results the pitch fibre CMC material does not fulfil the expectations for the targeted application to reduce local hot spots at high temperatures. It has to be carefully evaluated if the increased thermal conductivity of the CMC by a factor of 3-4 justifies the use for alternative objectives because of the high cost of the pitch fibres.

On the other hand, the mechanical properties of the pitch fibre CMC were surprisingly good as detailed in [11] and at least on the same level as those of the standard C/C-SiC material. So, the combination of good mechanical properties and an increased thermal conductivity at low temperature together with the low density of the material of 1.9 g/cm³ may present a case for certain design cases where just that increase in conductivity is required to have the solution of the problem but that has always to be investigated for the specific case.

11. REFERENCES

1. Eggers, T., Longo, J.M.A., Turner, J., Jung, W. Hörschgen, M., Stamminger, A., Gülhan, A., Siebe, F., Requardt, G., Laux, T., Reimer, T., Weihs, H. (2006). The SHEFEX Flight Experiment – Pathfinder Experiment for a Sky Based Test Facility. In Proc. 14th AIAA/AHI Space Planes and Hypersonic Systems and Technologies Conference, AIAA 2006-7921.

2. Bertin, J. J. (1993). Hypersonic Aerothermo-dynamics, AIAA, ISBN 978-1563470363.

3. Curry, D.M., Rochelle, W.C., Chao, D.C., Ting, P.C. (1986). Space Shuttle Orbiter Nose Cap Thermal Analysis, AIAA-86-0388.

4. Weihs, H., Hald, H., Reimer, T., Fischer, I. (2001). Development of a CMC Nose Cap for X-38. In Proc. IAF-01-I.3.01, 52nd International Astronautical Congress, Toulouse, France.

5. Johnson, S., Gasch, M., Stackpoole, M., Lawson, J., Gusman, M. (2009). Recent Developments in Ultra High Temperature Ceramics at NASA Ames. In Proc. 16th AIAA International Space Planes and Hypersonic Systems and Technologies Conference, AIAA 2009-7219.

6. Kolodziej, P., Bull, J., Salute, J., Keese, D.L. (1995). First Flight Demonstration of a Sharp Ultra-High Temperature Ceramic Nosetip. NASA TM-112215

7. Böhrk, H. (2014). Transpiration Cooling at Hypersonic Flight – AKTiV on SHEFEX II. In Proc. 11th AIAA/ASME Joint Thermophysics and Heat Transfer Conference, AIAA 2014-2676.

8. Krenkel, W.(2005). *Carbon Fiber Reinforced Silicon Carbide Composites (C/SiC, C/C-SiC), Handbook of Ceramic Composites*, Kluwer Academic Publishers, NL

9. Chand, S. (2000). Review Carbon fibers for composites. *J. Materials Sci.*. **35**, 1303-1313

10. Fitzer, E. (1989). *Pan-based carbon fibers – present state and trend of the technology from the viewpoint of possibilities and limits to influence and to control the fiber properties by the process parameters*. Carbon, **27**(5), 621-645

11. Reimer, T., Petkov, I., Koch, D., Frieß, M., Dellin, C. (2014). *Fabrication and Characterization of C/C-SiC Material made with Pitch-Based Carbon Fibers*. In Proc. Material Science and Technology 2014, Pittsburgh, USA

12. Sippel, M., van Foreest, A., Bauer, C. (2011). System Investigations of the SpaceLiner Concept in FAST20XX. In Proc. 17th AIAA Space Planes and Hypersonic Systems and Technologies Conference, AIAA 2011-2294.